Modal oscillation control in internally patterned $Ni_{80}Fe_{20}$ thin film microstructures

M. Belov, Z. Liu, R. D. Sydora, and M. R. Freeman
Department of Physics, University of Alberta, Edmonton, AB T6G 2J1, Canada
(Received 10 September 2003; published 17 March 2004)

The broadband magnetization dynamics (MD) of lithographic, polycrystalline thin film ferromagnetic $Ni_{80}Fe_{20}$ elements is studied experimentally using time-resolved scanning Kerr microscopy and numerically via micromagnetic simulation. The spatiotemporal evolution of the polar component of magnetization in response to a small out-of-plane transient magnetic pulse is imaged in the presence of a weak in-plane static bias field. In a uniform square platelet the spatial response is strongly controlled by the nonuniform static magnetization distribution associated with the closure domains transverse to the bias field direction. A circular pinhole is patterned in the center of a square platelet to show that the spatial pattern of magnetization oscillation response also depends sensitively on weaker variations of the static magnetization. The Landau Lifshitz Gilbert model reproduces the observed modal oscillation symmetry and reveals in detail that the observation of spatially nonuniform damping in the experiment is a result of conversion of energy into shorter wavelength modes in the vicinity of the domain boundaries.

DOI: 10.1103/PhysRevB.69.094414 PACS number(s): 75.30.Ds, 76.50.+g, 75.40.Gb, 75.75.+a

I. INTRODUCTION

Current studies of micromagnetic structures in the subnanosecond temporal regime have been stimulated by interests in high speed information storage and spintronic applications. The physics of magnetic thin films, especially when microscopically shaped, is complicated and a comprehensive understanding of relaxation mechanisms[1–3] requires extensive study on both microscopic and sub nanosecond scales.[4–6] The collective modes or spin waves of patterned magnetic thin films have been studied intensively using ferromagnetic resonance[7–11] and Kerr microscopy,[12–19] Brillouin light spectroscopy,[20–23] inductive detection,[24,25] and magnetic force microscopy.[26–28] Recent results show that the geometrical form of ultrathin magnetic films together with ultrafast magnetic excitation can significantly affect the oscillations of the direction of a magnetization vector.[16,17,30] Further comparison of experimental results with numerical simulations based on solutions of the Landau-Lifshitz-Gilbert (LLG) equation show in greater detail how the competition between exchange, self-magnetostatic, anisotropy, and external field energies controls magnetization excitations on small length and short time scales. In this work, the results of ultrafast stroboscopic scanning Kerr microscopy experiments and numerical simulations on two related classes of micrometer-scale thin film element are presented. Two square samples are investigated, with and without a small circular pinhole defect in the center. Significant changes in both spatial and temporal characteristics of broadband magnetization dynamics response owing to the defect are shown and discussed.[29]

The samples were fabricated from 15-nm-thick polycrystalline $Ni_{80}Fe_{20}$ films deposited by dc magnetron sputtering onto a sapphire substrate and patterned using electron beam lithography and lift-off (with two-layer resist process). Figure 1 shows an optical micrograph of a specimen hosting a family of independent elements, and a scanning electron micrograph ''close-up'' of the 4 ± 0.05-μm square with a 240 ±10-nm-diameter central pinhole investigated in this study. The structures are within an elongated loop of 300 ± 15-nm-thick, 20 ± 0.25-μm-wide gold wire (patterned in an initial process of optical lithography and wet chemical etching), which carries the fast current pulses. The measurements are performed by a conventional pump-probe optical method, using 100 femtosecond pulses from an 80-MHz mode-locked Ti:sapphire oscillator tuned to 780 nm. The relative timing of the 10-mW pump beam is controlled by a variable optical delay line, and intensity modulated by a 1-kHz chopper before focusing onto a fast photodiode that generates a 40-mA current pulse. The resulting out-of-plane transient magnetic field of magnitude 637 A/m (computed using the Biot-Savart method) and rise time 200 ps ($\pm10\%$) is useful for broadband excitation of oscillations over a bandwidth of several GHz. The sample is biased along the x direction by an external dc magnetic field. A 1-mW linearly polarized probe beam is focused onto the surface of the magnetic microstructure using a 0.9 numerical aperture microscope objective. The waist size of the beam at the sample (Airy formula) is 0.5 μm based on the 1-mm radius of the objective's aperture and the uniform distribution of the optical beam intensity profile (initially 2 mm in diameter, the beam was expanded five times). Measurement of the (polar) Kerr component[12–14] of the reflected optical signal is accomplished through polarization analysis by a Thompson prism,

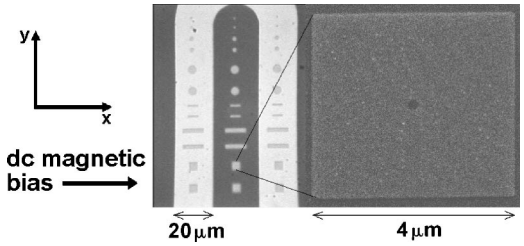

FIG. 1. Optical (left) and electron microscopy images of the sample structure, with the coordinate system for the field geometry. The transient out-of-plane field is generated by current flow through the elongated gold loop (bright in the optical image).

two detectors with integrated amplifiers, a differential preamp, and a lock-in amplifier.[11]

II. SIMULATION

To compare experimental results with the simulations the temporal profile of the magnetic excitation (pumping) from the transmission line was extracted from magnetization dynamics curve [the magnetization oscillations at a dc bias field of 80 kA/m ($\pm 5\%$) taken from the center of the sample]. The filtering process was accomplished by a Fourier transform of the magnetization dynamics curve, cutting off the high frequency magnetization oscillations and leaving the Fourier components related to the pumping pulse only. After a final backward Fourier transform into time domain the resulting data [see the inset in Fig. 2(a)] were used in the numerical computation as a definition of the external excitation. Due to electrical reflections several additional peaks with smaller amplitudes propagate through the Au transmission line. The following parameters were used in the LLG equation: exchange constant 1.05×10^{-11} J/m, saturation magnetization 57 kA/m, anisotropy field 478 A/m, dimensionless damping constant 0.013 (0.5 for initial state computation), and a lateral cell size of 7.8 nm (512×512 grid). Some simulation data were processed by convolution with a Gaussian kernel of width 425 nm to mimic the experimental view, albeit at slightly higher spatial resolution.

III. EXPERIMENT AND DISCUSSION

The oscillations of the polar component of magnetization measured at the center of the uniform (no central pinhole) sample, normalized to the height of the initial peak, are shown in Fig. 2(a) (symbols) together with the numerical LLG curve (solid line). The first peak of the magnetization dynamics curve includes the parametric response to the excitation pulse, and the height of this peak relative to the amplitude of the subsequent oscillations is very sensitive to the excitation pulse shape. In the parametric contribution the direction of the magnetization vector is controlled by low (below the resonance) frequency components of the Fourier spectra of the excitation pulse. The slight discrepancy in peak levels in the comparison between experiment and model for the first series of oscillations is attributable to a small difference in shape between the actual transient magnetic pulse and the one extracted from the magnetization dynamics curve at a dc bias of 80 kA/m.

For low amplitude transient excitations, the closure domain structures yield an essentially static, spatially nonuniform magnetization and effective field that plays a dominant role both in the initial response and subsequent small angle evolution of the magnetization. Two-dimensional images of the polar magnetization change across the entire uniform specimen are shown in the lower panels of Fig. 2(b), for two different instants during the first cycle of oscillation. At 225 ps ($\pm 5\%$), on the initial peak, a strong spatial contrast has developed along the closure domain boundaries (the static magnetization is arranged in a ''C'' state) with an inclination towards $+y$ and $-y$ in the left and right closure domains,

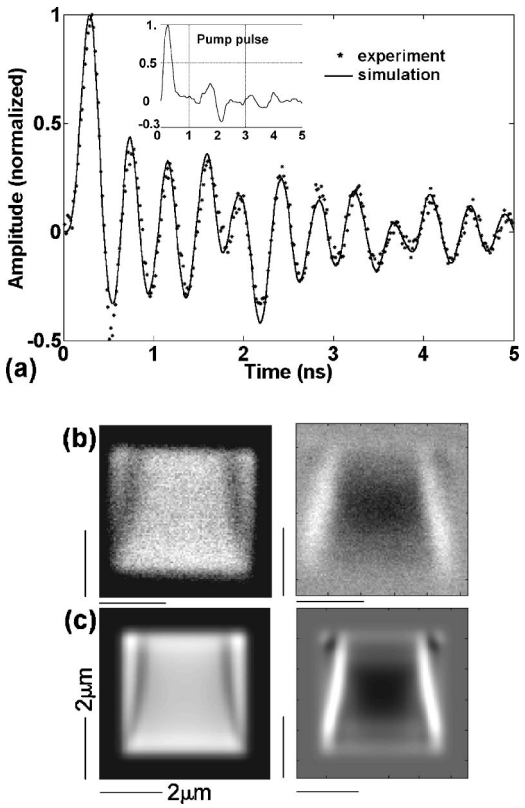

FIG. 2. The local response of the polar component of the magnetization at the center of the platelet for static magnetic field 4.6 kA/m (*line), and corresponding numerical simulation (solid line) are shown in (a) together with the experimental (b) and numerical (c) spatial images at 225 ps (left) and 450 ps (right) from the start of magnetic excitation. Cell size in simulation [(c), left] and [(c), right] was 15.6 and 7.8 nm, respectively. Scale line is 2 μm. The maximum (white) corresponds to the 0.1° angle of the polar component of the magnetization.

respectively, while the central magnetization is along $+x$ (horizontal axis). The response is unipolar here, and the gray scale such that black corresponds to no change (witness the border around the specimen.) Hence by the time the central magnetization has reached its initial peak, there has yet to be significant change along the domain boundaries. Qualitatively, the response of a uniform magnetization, having a well-defined frequency of the oscillations, to a broadband pulsed excitation can be visualized by separating the spectral content of the excitation into three frequency bands. The magnetization (by its ''slow'' frequency content in the Fourier domain) parametrically follows the excitation field, below the resonance frequency. The frequency content overlapping the ferromagnetic resonance frequency peak couples to the resonance, causing an initial precession of the magnetization about the excitation field axis (resultant field in the rotating frame) and hence an initial change of magnetization vector orthogonal to the parametric response, while the response to higher frequencies is attenuated. The relative delay of the polar magnetization response at the closure domain boundaries implies a lower local resonant frequency and proportionally stronger resonant response at those locations. The 4-μm scale of these structures is large enough that such a

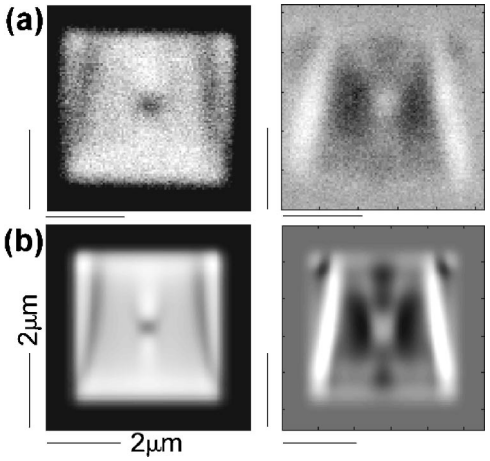

FIG. 3. The experimental (a) and simulation (b) spatial images of polar component of the magnetization responses at 225 ps (left) and 450 ps (right) from the start of magnetic excitation. The 4.6-kA/m dc bias field direction is parallel with the horizontal axis of the squares. The sample with the central pinhole is on the right. The simulated images were blurred by convolution with a Gaussian kernel. The scale line is 2 μm.

decomposition of the initial response into locally different behaviors is still viable. Recognizing that the eigenmodes of the system have a hybridized character combining magnetostatic and spin wave characteristics.[16,17,22,23] it is nevertheless possible to distinguish the magnetostaticlike and spin-wavelike excitations, existing on well-separated length scales in this geometry, and to observe their interactions in the regions of spatially nonuniform magnetization (below).

When a submicrometer pinhole is patterned in the center of the platelet, the static magnetization accommodates itself to the change by forming cusp-like structures at the edges of the hole normal to the bias field direction, in effect allowing the magnetization to streamline around the hole. Such structures have been imaged by magnetic force microscopy for larger holes in permalloy films.[26] This has an interesting consequence for the magnetization dynamics response. Whereas the formerly uniform magnetization in the center of the platelet presented a flat effective field for a uniform mode of oscillation, the new ''potential surface'' has a quadrupolar variation as a function of angle about the center. The dominant spatial mode excited by the broadband magnetization excitation reflects this symmetry, seen clearly in Fig. 3 for both the experimental measurements and the micromagnetic simulations. Note, in comparison with Fig. 2, that the other spatial features associated with the closure domains are identical, with and without a central pinhole.

A ''one-dimensional movie'' of the response is obtained from assembling horizontal cross-section or line-scan measurements for a high density of time sampling points into single two-dimensional images, as in Fig. 4. These ''x vs t'' renderings of the signal provide additional insight into evolution of the nonequilibrium magnetization.[16,17] A striking feature of these images is the apparent spatially non-uniform damping of the modal oscillation in the central domain. The situation represents a cleanly realized case in point of the notion of indirect damping of magnetization oscillations.[4]

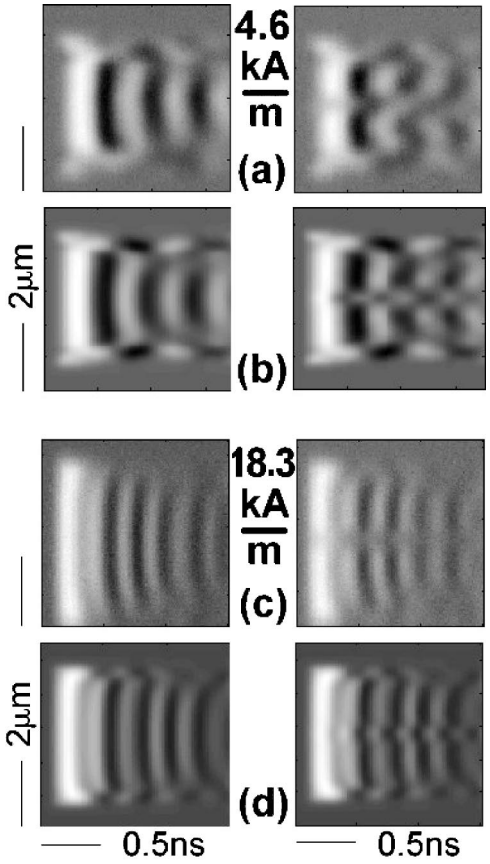

FIG. 4. Spatiotemporal images of polar component of the magnetization dynamic responses from the experiment [(a) and (c)] and LLG equation [(b) and (d)] at, dc bias 4.6 kA/m [(a) and (b)] and 18.3 kA/m [(c) and (d)] based on ''x vs t'' signal rendering. The experimental cross-section, a 40 nm step scanning line through the center of the platelet, is parallel with the dc bias field direction. The sample with the defect is on the right. The compilation of successive snapshots was obtained using 12-ps steps and simulation data were processed by convolution with a Gaussian kernel. Spatial and temporal scale lines are 2 μm and 0.5 ns respectively.

The nonuniform magnetization at the closure domain boundaries gives rise to magnon-magnon scattering,[4–6] converting energy from the ''uniform'' (longer wavelength) mode of the central domain into shorter spin waves where it disappears below the spatial resolution of the measurement. Turning off the Gaussian blur of the simulation makes this process very clear. Additional magnons are launched from the non-

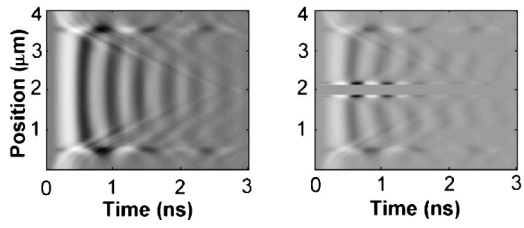

FIG. 5. Spatiotemporal evolution of magnon-magnon scattering at a dc bias of 4.6 kA/m extracted from the numerical solution of the LLG equation. The data were not processed by convolution with a Gaussian kernel.

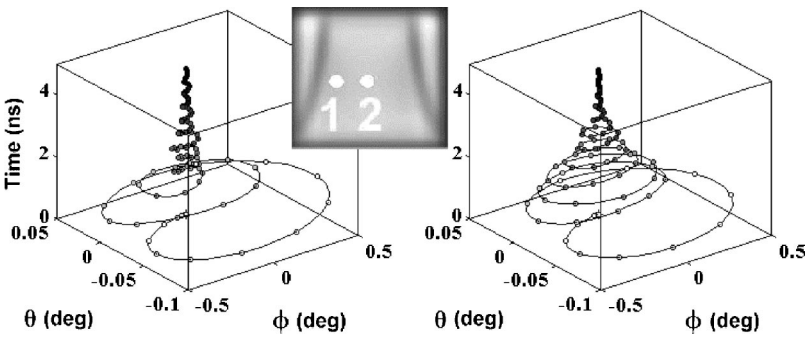

FIG. 6. Full trajectories of the small-angle changes in orientation of the magnetization vector at two different points of the platelet (1, a micron from the left edge, and 2, at the center). The spherical coordinates (delta ϕ is in the plane of the specimen and delta θ is perpendicular to it) were taken from simulations with a dc bias field of 4.6 kA/m.

uniform magnetization around the pinhole resulting in ''double-*V*'' *x*-*t* profile. Figures 4(c) and 4(d) (right) show that the magnetization at a dc bias of 18.3 kA/m (with an ''*S*'' initial state) is sufficiently uniform near the hole, and, consequently, the magnon-magnon scattering is suppressed relative to that caused near the closure domains. Spatiotemporal responses extracted from non-convoluted numerical data at a dc bias of 4.6 kA/m are shown in Fig. 5 (with the results from the sample with a defect on the right). The energy of the ''uniform'' mode is converted to shorter wavelength modes by magnon-magnon scattering in the nonuniform effective field near the domain boundary and around the pinhole (right). The influence of this interaction propagates across the specimens, with and without the defect, at spin-wave velocities of 850 and 610 m/s, respectively (these values were measured from experimental ''*x* vs *t*'' renderings not displayed here). Corresponding values from the simulation are 800 and 590 m/s (within $\pm 10\%$ error range for both the experimental and simulation velocity values). The short wavelength modes are below the spatial resolution of our microscope, giving rise to a characteristic ''*V*''-shaped envelope as they propagate towards the center of the specimen at constant speed. Although position dependent, the apparent relaxation of precessional oscillation is accelerated everywhere in the sample as a result of this indirect damping due to magnon-magnon scattering along the domain boundaries.

The temporal changes of the full magnetization vector (trajectory of in-plane and out-of-plane angles versus time) at two locations are illustrated in Fig. 6, from a LLG simulation (assuming a reflection-free pulse for clarity). A characteristic disruption of the magnetization oscillations is seen at time 1.2 ns in the left panel, corresponding to a position 1 μm left of center. In contrast, the precession decays smoothly at the center of the specimen during the entire time interval shown.

IV. CONCLUSION

A spatiotemporal study of broadband magnetization dynamics in internally patterned thin film permalloy platelets was conducted in order to elucidate the excitation and decay of modal oscillations in microstructures. It was shown that the primary mode of magnetization oscillations in the center of the platelet biased in a weak longitudinal field adapts to the configuration of static magnetization, assuming a quadrupolar pattern around a small pinhole defect. Moreover, the comparison with micromagnetic simulation highlights the results as a clear case in point for the concept of ''indirect damping.'' The transfer of energy into shorter wavelength modes by magnon-magnon scattering in regions of nonuniform magnetization is responsible for the appearance of position-dependent decay of oscillations in the measurement. The work is a step towards a more elaborate manipulation of allowed magnetic modes, or ''magnonics.'' Continuing studies of these ferromagnetic ''ripple tanks'' will explore the influence of patterns of multiple defects, and the amplitude dependent response in this intrinsically nonlinear system. Spatial control of modal oscillations is also potentially of interest for applications in magnetic logic.

ACKNOWLEDGMENTS

The samples were prepared in the University of Alberta Nanofab (www.nanofab.ualberta.ca), and the simulations run on resources of MACI (www.maci.ca) using an evolution of micromagnetics code originally written by A. Stankiewicz and G. Ballentine. We thank NSERC and iCORE for financial support, and CIAR for inspiration. M.B. is grateful to JDS Uniphase for a Graduate Scholar award.

[1] Ch. Kittel, Phys. Rev. **73**, 155 (1948).
[2] L.R. Walker, Phys. Rev. **105**, 390 (1957).
[3] R.W. Damon and J.R. Eshbach, J. Phys. Chem. Solids **19**, 308 (1961).
[4] E.D. Boerner, H. Neal Bertram, and H. Suhl, J. Appl. Phys. **87**, 5389 (2000).
[5] V. Kambersky and C.E. Patton, Phys. Rev. B **11**, 2668 (1975).
[6] H. Suhl, J. Appl. Phys. **89**, 7448 (2001).
[7] S. Tamaru, J.A. Bain, R.J.M. van de Veerdonk, T.M. Crawford, M. Covington, and M.H. Kryder, J. Appl. Phys. **91**, 8034 (2002).
[8] R.J. Hicken and J. Wu, J. Appl. Phys. **85**, 4580 (1999).
[9] J. Wu, N.D. Hughes, J.R. Moore, and R.J. Hicken, J. Appl. Phys. **89**, 6692 (2001).
[10] M. van Kampen, C. Jozsa, J.T. Kohlhepp, P. LeClair, L. Lagae, W.J.M. de Jonge, and B. Koopmans, Phys. Rev. Lett. **88**, 227201 (2002).
[11] M.R. Freeman and J.F. Smyth, J. Appl. Phys. **79**, 5898 (1996).
[12] P.N. Argyres, Phys. Rev. **97**, 334 (1955).

[13] M. Mansuripur, J. Appl. Phys. **67**, 6466 (1990).
[14] J. Zak, E.R. Moog, C. Liu, and S.D. Bader, Phys. Rev. B **43**, 6423 (1991).
[15] W.K. Hiebert, A. Stankiewicz, and M.R. Freeman, Phys. Rev. Lett. **79**, 1134 (1997).
[16] J.P. Park, P. Eames, D.M. Engebretson, J. Berezovsky, and P.A. Crowell, Phys. Rev. Lett. **89**, 277201 (2002).
[17] J.P. Park, P. Eames, D.M. Engebretson, J. Berezovsky, and P.A. Crowell, Phys. Rev. B **67**, 020403 (2003).
[18] Y. Acremann, C.H. Back, M. Buess, O. Portmann, A. Vaterlaus, D. Pescia, and H. Melchior, Science **290**, 492 (2000).
[19] Th. Gerrits, J. Hohlfeld, O. Gielkens, K.J. Veenstra, K. Bal, Th. Rasing, and H.A.M. van den Berg, J. Appl. Phys. **89**, 7648 (2001).
[20] J. Jorzick, S.O. Demokritov, C. Mathieu, B. Hillebrands, B. Bartenlian, C. Chappert, F. Rousseaux, and A.N. Slavin, Phys. Rev. B **60**, 15 194 (1999).
[21] S.O. Demokritov, B. Hillebrands, and A.N. Slavin, Phys. Rep. **348**, 441 (2001).
[22] J. Jorzick, S.O. Demokritov, B. Hillebrands, M. Bailleul, C. Fermon, K.Y. Guslienko, A.N. Slavin, D.V. Berkov, and N.L. Gorn, Phys. Rev. Lett. **88**, 047204 (2002).
[23] A. Barman, V.V. Kruglyak, R.J. Hicken, A. Kundrotaite, and M. Rahman, Appl. Phys. Lett. **82**, 3065 (2003).
[24] M. Grimsditch, Y. Jaccard, and I.K. Schuller, Phys. Rev. B **58**, 11539 (1998).
[25] M. Covington, T.M. Crawford, and G.J. Parker, Phys. Rev. Lett. **89**, 237202 (2002).
[26] T.M. Crawford, M. Covington, and G.J. Parker, Phys. Rev. B **67**, 024411 (2003).
[27] C. Merton, G.D. Skidmore, J. Schmidt, E.D. Dahlberg, H. Wan, and B. Pant, J. Appl. Phys. **85**, 4601 (1999).
[28] T. Shinjo, T. Okuno, R. Hassdorf, K. Shigeto, and T. Ono, Science **289**, 931 (2000).
[29] A. Fernandez and C.J. Cerjan, J. Appl. Phys. **87**, 1395 (2000).
[30] K. Yu Guslienko, R. W. Chantrell, and A. N. Slavin, Phys. Rev. B **68**, 024422 (2003).